

Polarized States and Domain Walls in Spinor Bose-Einstein Condensates

H. E. Nistazakis,¹ D. J. Frantzeskakis,¹ P. G. Kevrekidis,² B. A. Malomed,³ R. Carretero-González,⁴ and A. R. Bishop⁵

¹*Department of Physics, University of Athens, Panepistimiopolis, Zografos, Athens 15784, Greece*

²*Department of Mathematics and Statistics, University of Massachusetts, Amherst MA 01003-4515, USA*

³*Department of Interdisciplinary Studies, Faculty of Engineering, Tel Aviv University, Tel Aviv 69978, Israel*

⁴*Nonlinear Dynamical Systems Group, Department of Mathematics and Statistics, and Computational Science Research Center, San Diego State University, San Diego CA, 92182-7720, USA*

⁵*Theoretical Division and Center for Nonlinear Studies, Los Alamos National Laboratory, Los Alamos, New Mexico 87545, USA*

We study spin-polarized states and their stability in anti-ferromagnetic states of spinor ($F = 1$) quasi-one-dimensional Bose-Einstein condensates. Using analytical approximations and numerical methods, we find various types of polarized states, including: patterns of the Thomas-Fermi type; structures with a pulse-shape in one component inducing a hole in the other components; states with holes in all three components; and domain walls. A Bogoliubov-de Gennes analysis reveals that families of these states contain intervals of a weak oscillatory instability, except for the domain walls, which are always stable. The development of the instabilities is examined by means of direct numerical simulations.

I. INTRODUCTION

The development of the far-off-resonant optical techniques for trapping ultracold atomic gases has opened new directions in the studies of Bose-Einstein condensates (BECs). Atoms can be confined regardless of their hyperfine (spin) state, thus avoiding freezing the atom's spin degree of freedom, making it available for the study of interesting spin dynamics [1]. One of the major achievements in this direction was the experimental creation of *spinor* BECs [2, 3]. The spinor condensate formed by atoms with spin F is described by a $(2F+1)$ -component macroscopic (mean-field) wave function, which gives rise to various phenomena that are not present in single-component BECs, including formation of spin domains [4], spin textures [5], and multi-component (vectorial) solitons of bright [6, 7, 8], dark [9], gap [10] and bright-dark [11] types.

Generally, the dynamics of the spinor $F = 1$ BEC is spin-mixing [12]. However, there also exist non-mixing, or *spin-polarized* states of the system, which are stationary solutions of the corresponding system of Gross-Pitaevskii (GP) equations [13, 14]. The stability of such polarized states is different for the two distinct types of the $F = 1$ condensates, namely the *ferromagnetic* (FM), such as in ^{87}Rb , and *polar* (alias *anti-ferromagnetic*, AFM), such as ^{23}Na , ones, where the spin-dependent interactions are, respectively, attractive and repulsive. Accordingly, as demonstrated in Ref. [15] (see also Ref. [7]), spin-polarized states are modulationally stable/unstable in the AFM/FM condensates.

In this work, we focus on AFM spinor condensates, and study, in particular, spin-polarized states of the spinor BEC of ^{23}Na atoms. Assuming that this spinor system is confined in a strongly anisotropic trap, we first present the respective system of three coupled quasi one-dimensional (1D) GP equations. Then, employing the so-called single-mode approximation [12, 15], we use analytical and numerical methods to find the spin-polarized

states of the system and study their stability via the Bogoliubov-de Gennes (BdG) equations (i.e., the linearization of the GP equations). The simplest possible form of these states are the stable Thomas-Fermi (TF) configurations (for each hyperfine component). We also present other spin-polarized states, including ones in which one component maintains a pulse-like shape, inducing a hole in the other components, and structures with holes in all the three components. All these states feature instability regions too, but with values of the normalized instability growth rate up to $\sim 10^{-3}$. Development of the oscillatory instabilities is examined by means of direct simulations. It is found that the structures with a hole in one component get weakly deformed, while the states with holes in all the three components suffer stronger deformations. If the three components are initially spatially separated, being confined in different harmonic traps, but are put in a single trap afterwards, spin domain-wall (DW) patterns are formed. A family of the DW solutions exists and is fully stable if, for a fixed value of the trap's strength, the chemical potential (or the number of atoms) exceeds a certain critical value.

The paper is organized as follows: Section II presents the model. Sections III is dealing with TF states. In Sections IV and V we examine structures with one and multiple holes, respectively (including their stability). Finally, conclusions are presented in Section VI.

II. THE MODEL AND SETUP

At sufficiently low temperatures, and in the framework of the mean-field approach, a spinor BEC with $F = 1$ is described by a vectorial order parameter, $\Psi(\mathbf{r}, t) = [\Psi_{-1}(\mathbf{r}, t), \Psi_0(\mathbf{r}, t), \Psi_{+1}(\mathbf{r}, t)]^T$, with the different fields corresponding to three values of the vertical component of the spin, $m_F = -1, 0, +1$. Assuming that this condensate is loaded into a strongly anisotropic trap, with holding frequencies $\omega_x \ll \omega_{\perp}$, we assume, as usual, that the

wave functions are separable, $\Psi_{0,\pm 1} = \psi_{0,\pm 1}(x)\psi_{\perp}(y, z)$, where the transverse components $\psi_{\perp}(y, z)$ represent the ground state of the respective harmonic oscillator. Then, following the standard approach [16] of averaging the coupled 3D GP equations for the three components in the transverse plane (y, z) , leads to the system of coupled 1D equations for the longitudinal components of the wave functions (see Refs. [6, 7, 9, 10, 11]):

$$i\hbar\partial_t\psi_{\pm 1} = \hat{H}_{\text{si}}\psi_{\pm 1} + c_2^{(1D)}(|\psi_{\pm 1}|^2 + |\psi_0|^2 - |\psi_{\mp 1}|^2)\psi_{\pm 1} + c_2^{(1D)}\psi_0^2\psi_{\mp 1}^*, \quad (1)$$

$$i\hbar\partial_t\psi_0 = \hat{H}_{\text{si}}\psi_0 + c_2^{(1D)}(|\psi_{-1}|^2 + |\psi_{+1}|^2)\psi_0 + 2c_2^{(1D)}\psi_{-1}\psi_0^*\psi_{+1}, \quad (2)$$

where star denotes complex conjugate, and $\hat{H}_{\text{si}} \equiv -(\hbar^2/2m)\partial_x^2 + (1/2)m\omega_x^2x^2 + c_0^{(1D)}n_{\text{tot}}$ is the spin-independent part of the Hamiltonian, with $n_{\text{tot}} = |\psi_{-1}|^2 + |\psi_0|^2 + |\psi_{+1}|^2$ being the total density (m is the atomic mass). The nonlinearity coefficients have an effectively 1D form, namely $c_0^{(1D)} = c_0/2\pi a_{\perp}^2$ and $c_2^{(1D)} = c_2/2\pi a_{\perp}^2$, where $a_{\perp} = \sqrt{\hbar/m\omega_{\perp}}$ is the transverse harmonic-oscillator length which determines the size of the transverse ground state. Coupling constants c_0 and c_2 account for, respectively, the mean-field spin-independent and spin-dependent binary interactions between identical spin-1 bosons,

$$\{c_0, c_2\} = (4\pi\hbar^2/3m) \{(a_2 + a_0), (a_2 - a_0)\}, \quad (3)$$

where a_0 and a_2 are the s -wave scattering lengths in combined symmetric collision channels of total spin $f = 0, 2$. The spinor $F = 1$ condensate with $c_2 < 0$ and $c_2 > 0$ is, respectively, of the FM and AFM types, as, respectively, in ^{87}Rb and ^{23}Na [13, 17].

Measuring time, length and density in units of $\hbar/c_0^{(1D)}n_0$, $\hbar/\sqrt{mc_0^{(1D)}n_0}$ and n_0 (here, n_0 is the peak density), we cast Eqs. (1)-(2) in the dimensionless form,

$$i\partial_t\psi_{\pm 1} = H_{\text{si}}\psi_{\pm 1} + \delta(|\psi_{\pm 1}|^2 + |\psi_0|^2 - |\psi_{\mp 1}|^2)\psi_{\pm 1} + \delta\psi_0^2\psi_{\mp 1}^*, \quad (4)$$

$$i\partial_t\psi_0 = H_{\text{si}}\psi_0 + \delta(|\psi_{-1}|^2 + |\psi_{+1}|^2)\psi_0 + 2\delta\psi_{-1}\psi_0^*\psi_{+1}, \quad (5)$$

where $H_{\text{si}} \equiv -(1/2)\partial_x^2 + (1/2)\Omega_{\text{tr}}^2x^2 + n_{\text{tot}}$, the normalized trap's strength is

$$\Omega_{\text{tr}} = \frac{3}{2(a_0 + 2a_2)n_0} \left(\frac{\omega_x}{\omega_{\perp}} \right), \quad (6)$$

and the parameter δ is given by

$$\delta \equiv \frac{c_2^{(1D)}}{c_0^{(1D)}} = \frac{a_2 - a_0}{a_0 + 2a_2} \quad (7)$$

($\delta < 0$ and $\delta > 0$ correspond, respectively, to the FM and AFM spinor condensate). For spin-1 ^{87}Rb and ^{23}Na

atoms, this parameter is $\delta = -4.66 \times 10^{-3}$ [18] and $\delta = 3.14 \times 10^{-2}$ [19], respectively. Thus, in these physically relevant cases, δ is a fixed small parameter of the system.

Spin-polarized states of the system, characterized by a constant population of each spin component, can be found upon substitution

$$\psi_j = \sqrt{n_j(x)} \exp(i\theta_j - i\mu_j t), \quad j = -1, 0, +1, \quad (8)$$

where n_j and θ_j are densities and phases of the components, and μ_j are their chemical potentials. Substituting this in Eqs. (4) and (5), it is readily found that conditions for the existence of spin-polarized states are

$$2\mu_0 = \mu_{-1} + \mu_{+1}, \quad (9)$$

$$\Delta\theta \equiv 2\theta_0 - \theta_{+1} - \theta_{-1} = 0 \quad \text{or} \quad \pi. \quad (10)$$

Below, we assume that the chemical potentials of the components are equal, $\mu \equiv \mu_{-1} = \mu_0 = \mu_{+1}$. For analysis of the stability of a stationary spin-polarized state, $\Psi_{\text{sps}}(x) = [\tilde{\psi}_{-1}(x), \tilde{\psi}_0(x), \tilde{\psi}_{+1}(x)]^T$, we will perform linearization around the unperturbed spin-polarized state, assuming a perturbed solution,

$$\psi_j(x, t) = \left[\tilde{\psi}_j(x) + \epsilon \left(u_j(x)e^{-\lambda_j t} + v_j^*(x)e^{\lambda_j^* t} \right) \right] e^{-i\mu t}, \quad (11)$$

where u_j and v_j represent infinitesimal perturbations with eigenvalues $\lambda \equiv \lambda_r + i\lambda_i$. Then, the solution of the ensuing linear-stability problem (i.e., the BdG equations) for λ and associated eigenfunctions u_j, v_j^* provides complete information about the stability of the underlying stationary state, Ψ_{sps} . Whenever it is unstable, we will also examine its evolution through direct simulations of GP equations (4) and (5), using a finite difference scheme in space and a fourth-order Runge-Kutta time integrator. Typically, in the simulations the unstable state is initially perturbed by a uniformly distributed random perturbation of relative amplitude 5×10^{-4} .

To estimate relevant physical parameters, we assume the spinor condensate of ^{23}Na atoms with peak 1D density $n_0 = 10^8 \text{ m}^{-1}$, confined in the harmonic trap with frequencies $\omega_{\perp} = 2\pi \times 230 \text{ Hz}$ and $\omega_x = 2\pi \times 13 \text{ Hz}$. In this case, the normalized trap strength is $\Omega = 0.1$ (this value is kept fixed throughout this work), while the number of atoms, N , depends on chemical potential μ and the particular form of spin-polarized states. Typically, we take μ in interval $1 \leq \mu \leq 5$, which corresponds to values of N in the range of $3.5 \times 10^3 \leq N \leq 3.5 \times 10^4$ atoms. For instance, at $\mu = 2$ the number of atoms is $N \sim 10^4$; in this case, the normalized time and space units correspond, respectively, to 1.2 ms and 1.83 μm .

III. THOMAS-FERMI SPIN-POLARIZED STATES

The simplest spin-polarized states can be found in the framework of the *single-mode approximation* [12, 15].

In anticipation, suggested by the approximation that components $\sqrt{n_j(x)}$ may be close to eigenmodes of a single effective potential, induced by the combination of the trap and nonlinearity, we introduce the ansatz $n_j(x) = q_j n(x)$, where coefficients q_j are the populations of each spin component in the steady state, related by the normalization condition, $q_{-1} + q_0 + q_{+1} = 1$. Then, Eqs. (4)-(5) lead to the following system:

$$\left[\hat{L} + \delta \left(1 + \sqrt{\frac{q_{\mp 1}}{q_{\pm 1}}} (sq_0 - 2\sqrt{q_{-1}q_{+1}}) \right) n \right] \sqrt{n} = 0, \quad (12)$$

$$\left[\hat{L} + \delta (1 - q_0 + 2s\sqrt{q_{-1}q_{+1}}) n \right] \sqrt{n} = 0, \quad (13)$$

where $\hat{L} \equiv -\mu - (1/2)\partial_x^2 + (1/2)\Omega^2 x^2 + n$ and $s = \pm 1$ for $\Delta\theta = 0$ or $\Delta\theta = \pi$, respectively. It is readily observed that the three equations (12), (13) are tantamount to a single one, viz.

$$\left(-\mu - \frac{1}{2}\partial_x^2 + \frac{1}{2}\Omega^2 x^2 + pn \right) \sqrt{n} = 0, \quad (14)$$

supplemented by relations

$$p \equiv 1 + \delta, \quad q_0 = 2\sqrt{q_{-1}q_{+1}} \quad \text{for } \Delta\theta = 0, \quad (15)$$

$$p \equiv 1, \quad q_{-1} = q_{+1} \quad \text{for } \Delta\theta = \pi. \quad (16)$$

In uniform space ($\Omega = 0$), Eq. (14) leads to the constant density, $n = \mu/p$. As shown in Refs. [7, 11, 15], such constant solutions to Eqs. (4)-(5) are modulationally stable only in the AFM phase, with $\delta > 0$. Below, we will only consider the case of the AFM condensate (in particular, bosonic sodium atoms with spin 1 and $\delta = 3.14 \times 10^{-2}$). In the presence of a sufficiently weak trap, Eq. (14) can be solved approximately employing the TF approximation [20]: neglecting the kinetic-energy term ($\sim \partial_x^2 \sqrt{n}$) in Eq. (14), we find density profiles of the three spin components: in the region where $\mu > (1/2)\Omega^2 x^2$,

$$n_j = \frac{q_j}{p} \left(\mu - \frac{1}{2}\Omega^2 x^2 \right), \quad (17)$$

and $n_j = 0$ elsewhere. Obviously, all three components of the TF solution have the same spatial width, or Thomas-Fermi radius, $R_{\text{TF}} = \sqrt{2\mu}/\Omega$.

In numerical simulations, we used a fixed-point algorithm (Newton-Raphson method) to find exact spin-polarized solutions to Eqs. (4)-(5), with profiles close to those produced by the TF approximation, as given by Eq. (17). In particular, we used, as an initial guess, three identical profiles of the form

$$\psi_j(x) = \sqrt{n(x)} \exp(i\theta_j), \quad (18)$$

with $n(x) = \mu - (1/2)\Omega^2 x^2$ and $\Delta\theta = 0$ or π . Then, keeping the trap's strength, Ω , fixed, we varied the chemical potential μ , and the numerical solution converged to stable spin-polarized states, which were indeed close to the

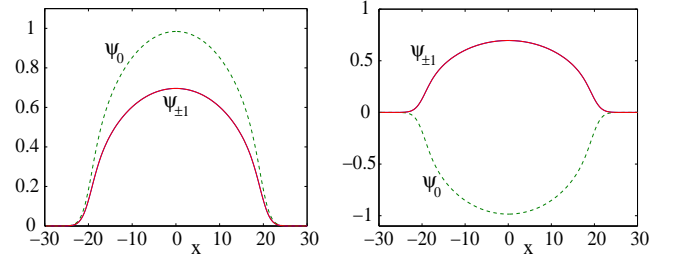


FIG. 1: (Color online) Examples of two stable spin-polarized states for $\Delta\theta = 0$ (left panel) and $\Delta\theta = \pi$ (right panel), both obtained for $\Omega = 0.1$ and $\mu = 2$. The wavefunctions $\psi_{\pm 1}$ are identical and are depicted by the solid line, while the wavefunction ψ_0 is depicted by the dashed line. In the left panel, $q_{-1} = q_{+1} = 0.5$ and $q_0 = 1$, while in the right panel $q_{-1} = q_{+1} = 0.25$ and $q_0 = 0.5$.

approximate one given by Eq. (17). Two typical examples are shown in the top panels of Fig. 1 for both cases, $\Delta\theta = 0$ (left panel) and $\Delta\theta = \pi$ (right panel), with $\Omega = 0.1$ and $\mu = 2$. The numerically determined states are very close to their TF-predicted counterparts, with $q_{-1} = q_{+1} = 0.5$ and $q_0 = 1$ ($\Delta\theta = 0$, left panel) and $q_{-1} = q_{+1} = 0.25$ and $q_0 = 0.5$ ($\Delta\theta = \pi$, right panel).

IV. SPIN-POLARIZED STATES WITH HOLES

Apart from the TF spin-polarized states, there exist other ones, which feature holes in some of the components. An example of such states is shown in Fig. 2. As seen in the two top panels of this figure (both a stable and an unstable state are shown—see below), the ψ_0 component is concentrated in the form of a pulse located at the trap's center, while the $\psi_{\pm 1}$ components feature a large hole at the same spot. This arrangement is explained by the fact that the interaction between components is repulsive, hence a peak (hole) in ψ_0 ($\psi_{\pm 1}$) induces a hole (peak) in $\psi_{\pm 1}$ (ψ_0). The norm N of each component is shown, as a function of chemical potential μ , in the third-row panel of Fig. 2. The set of the linear stability eigenvalues for this state is shown in the second-row panels of Fig. 2, for two different values of μ : The state with $\mu = 3$ (top-right) is stable, as all the eigenvalues are imaginary, while the state with $\mu = 2$ (top-left panel) is unstable. In fact, all such unstable states are destabilized by a Hamiltonian Hopf bifurcation, which leads to a quartet of eigenvalues with nonzero real parts. The instability interval is $1.81 \leq \mu \leq 2.15$, with the maximum instability growth rate $\text{Max}(\lambda_r) \approx 1.3 \times 10^{-3}$, found at $\mu \approx 2$ (see bottom panel of Fig. 2).

A similar state with the roles of $\psi_{\pm 1}$ and ψ_0 exchanged, i.e., the ψ_0 component featuring the hole, and $\psi_{\pm 1}$ ones concentrated in narrow pulses, were also found. Moreover, such states were found with either ψ_0 or $\psi_{\pm 1}$ having the opposite sign (i.e., for $\Delta\theta = \pi$). The results are not shown here, as the (in)stability of these states is qualita-

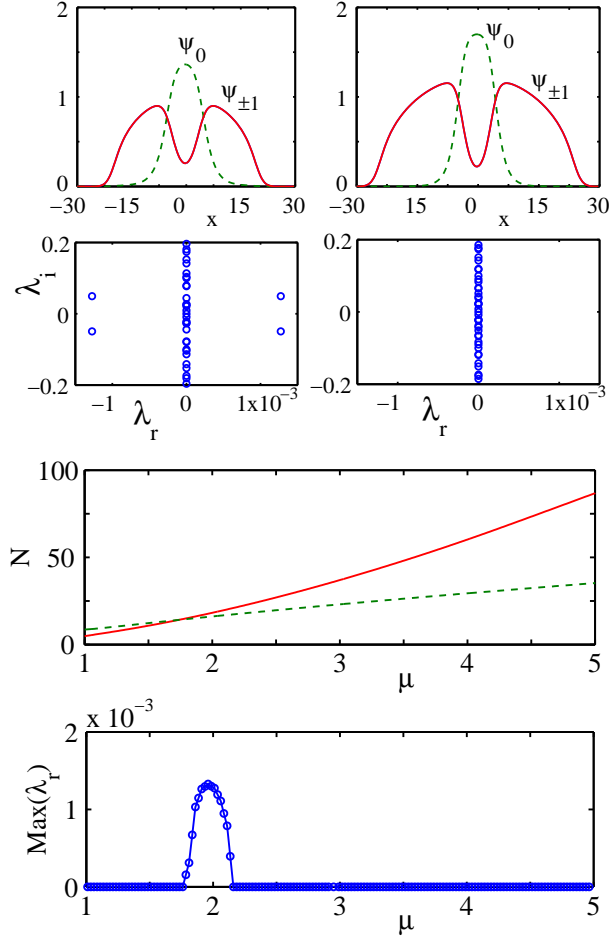


FIG. 2: (Color online) The spin-polarized state with a hole in each of the $\psi_{\pm 1}$ components, and a pulse-like ψ_0 component, for $\Omega = 0.1$ and $\Delta\theta = 0$. The two top left and right panels show unstable and stable states, with $\mu = 2$ and $\mu = 3$, respectively; solid and dashed lines depict the components $\psi_{\pm 1}$ and ψ_0 . The two panels in the second row display the spectral planes (λ_r, λ_i) of the (in)stability eigenvalues for the same states. Note that the instability (at $\mu = 2$) is of the oscillatory type, accounted for by a quartet of eigenvalues with nonzero real parts. The panel in the third row shows the normalized number of atoms (norm), N , of each component as a function of chemical potential μ ; solid and dashed lines show the norms of components $\psi_{\pm 1}$ and ψ_0 , respectively. The bottom panel shows λ_r as a function of μ , which reveals the instability window at $1.81 \leq \mu \leq 2.15$, with a maximum instability growth rate $(\lambda_r)_{\max} \approx 1.3 \times 10^{-3}$ at $\mu \approx 2$. The latter value corresponds to the unstable state shown in the top-left panel.

tively the same as in the above case.

The evolution of unstable states is exemplified in Fig. 3, which displays results of direct simulations of Eqs. (4) and (5) for the unstable state with $\Delta\theta = 0$ and $\mu = 2$, that was presented in Fig. 2 (top-left panel). In Fig. 3, contour plots of densities of the components of the solution are displayed as a function of time (the densities of the ψ_{+1} and ψ_{-1} components are identical).

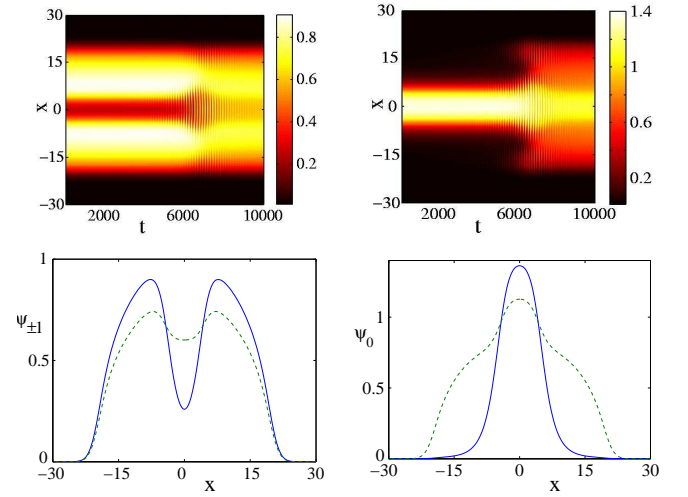


FIG. 3: (Color online) Top panels: Contour plots of densities of a solution shown in Fig. 2 subject to the oscillatory instability. The left and right panels display, respectively, identical densities of $\psi_{\pm 1}$ and that of ψ_0 . Because of the extremely small growth rate of the instability, it manifests itself only for $t > 4000$. Bottom panels: The respective wavefunction profiles at $t = 0$ (solid lines) and $t = 10000$ (dashed lines); as above, the left and right panels show, respectively, the wavefunctions $\psi_{\pm 1}$ and ψ_0 .

It is clearly observed that the predicted oscillatory instability sets in at a very large time ($t \approx 4000$, which corresponds to $t \approx 5$ seconds in physical units); this is a consequence of the extremely small growth rate of the instability. Eventually, the system settles down to a steady state, which has many similarities with the initial one. In particular, as seen in the top panels of Fig. 3, after $t \approx 8000$ the pulse in the ψ_0 component broadens and its amplitude is accordingly decreased, while the hole in the $\psi_{\pm 1}$ components becomes shallower. It is also noted that the three components develop a similar structure in their tails, as shown in the bottom panels of Fig. 3.

Apart from the states considered above, it is also possible to find spin-polarized states which feature, e.g., one hole in each of the $\psi_{\pm 1}$ components, and two holes in ψ_0 . Examples of such a state are shown in the top panels of Fig. 4 (the left one, for $\mu = 2$, is stable, while the right one, for $\mu = 3$ is unstable—see below). As seen in this figure, one may consider ψ_{-1} and ψ_{+1} as built of two overlapping pulses, which induce two holes in the ψ_0 component due to the repulsive interatomic interactions. Results of the stability analysis for these states are shown in Fig. 4. In this case, two quartets of eigenvalues with nonzero real parts are found in the spectral plane (see the second row right panel in Fig. 4) in the interval $2.58 \leq \mu \leq 3.22$ (the bottom panel in Fig. 4). The respective largest instability growth rate is $(\lambda_r)_{\max} \approx 1.8 \times 10^{-3}$ for $\mu \approx 2.9$, i.e., of the same order of magnitude as in the previous case. The development of the instability was studied, as above, in direct

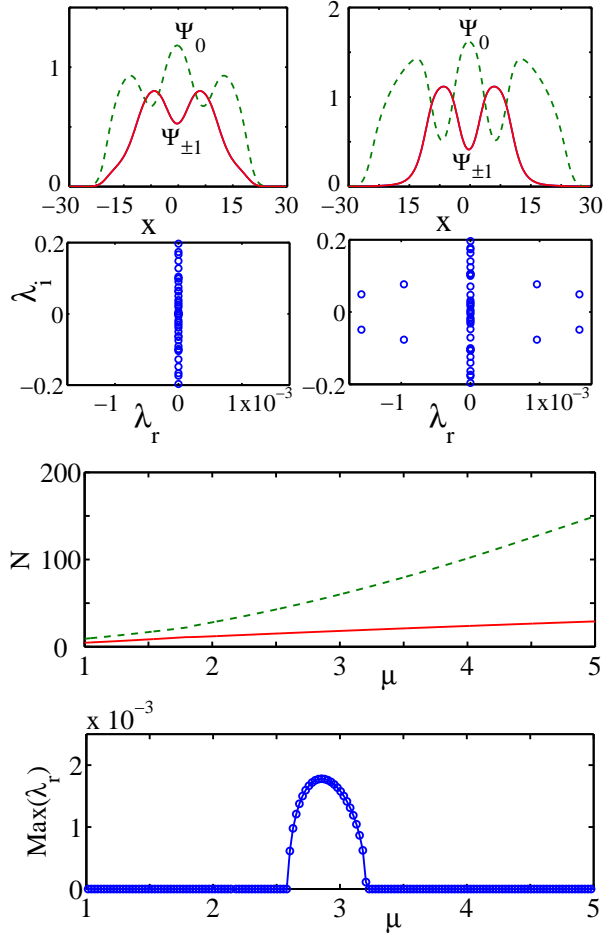


FIG. 4: (Color online) Same as Fig. 2 but for a state with one hole in each of the $\psi_{\pm 1}$ components and two holes in the ψ_0 component. In this case, the instability is manifested by two eigenvalue quartets the largest of which has a nonzero real part in the interval $2.58 \leq \mu \leq 3.22$; the maximum instability growth rate is $(\lambda_r)_{\max} \approx 1.8 \times 10^{-3}$ for $\mu \approx 2.9$. The unstable state shown in the top-right panel corresponds to $\mu = 3$.

simulations, starting with initial conditions in the form of a perturbed solution pertaining to $\mu = 3$. The result is shown in Fig. 5, in terms of the evolution of identical densities of the $\psi_{\pm 1}$ components, and the density of ψ_0 . Again, the instability manifests itself at large times ($t > 3500$, which corresponds to $t > 4.2$ seconds in physical units), but in this case the final result is a strong oscillatory deformation of the three spin components (after $t \approx 5500$), contrary to what is the case in Fig. 3 (the establishment of a new spin-separated state).

Similar states with one hole in ψ_0 and two holes in each of the $\psi_{\pm 1}$ components, as well their counterparts with $\Delta\theta = \pi$, have also been found. They are not shown here; as in the previous case, the (in)stability of these additional states is similar to that reported in Fig. 4.

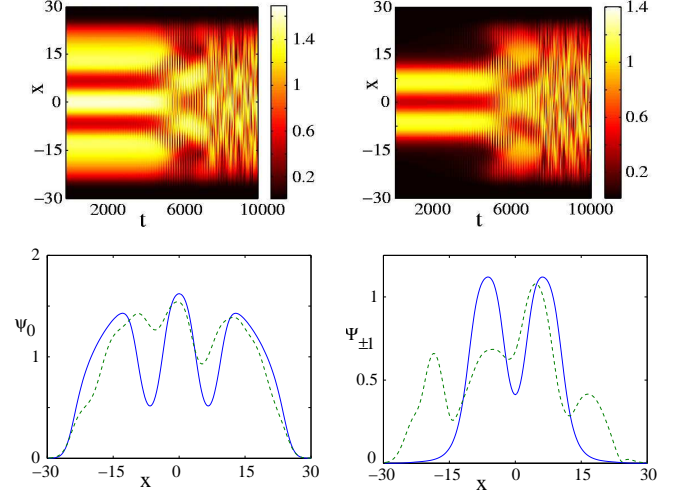


FIG. 5: (Color online) Same as Fig. 3, for the unstable state shown in the top-right panel of Fig. 4 (pertaining to $\mu = 3$). The instability manifests itself at large times ($t > 3500$) and results in strong oscillatory deformation of the clouds.

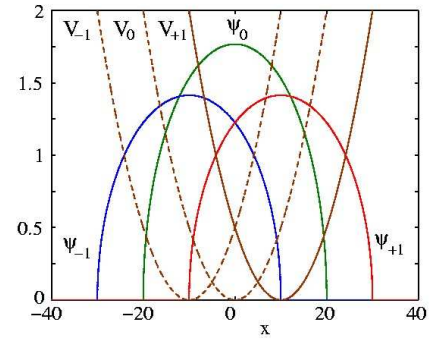


FIG. 6: (Color online) Initialization of the system when three different traps of the same strength but of different location are used: the TF clouds for ψ_{-1} , ψ_0 and ψ_{+1} are confined in harmonic traps of strength $\Omega = 0.1$ located, respectively, at $x = -10$, $x = 0$ (dashed lines) and $x = 10$ (solid line). The traps at $x = -10$ and $x = 0$ are turned off and this spinor configuration, confined solely in the trap located at $x = 10$, is introduced in the fixed-point algorithm.

V. DOMAIN WALLS

In the above sections, we reported the spin-polarized states in which all three spin components were spatially overlapping, since they were confined to the same potential trap. However, it is also possible to use three different traps, each confining a different component, to initially separate them, and then allow the system to evolve in the presence of one of these traps (i.e., turning off the other two). In this section, we present spin-polarized states, including DW structures, obtained in this way.

First, we describe the initialization of the system. We assume that the three TF-shaped components are ini-

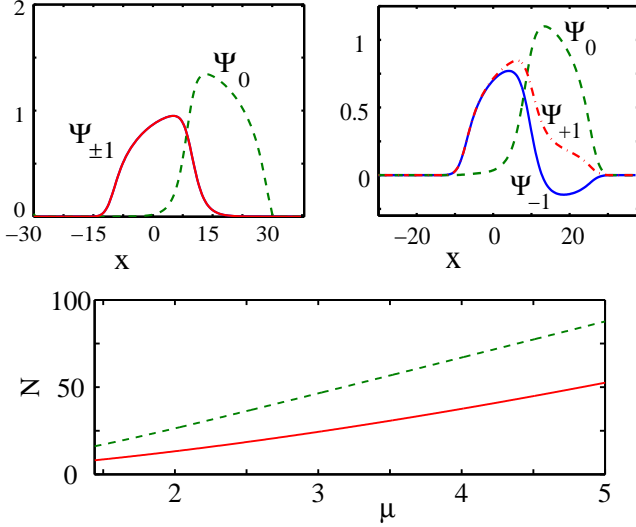


FIG. 7: (Color online) Top-left panel: the wave functions of the components (ψ_{+1} and ψ_{-1} are identical) in a stationary state found from the initial configuration prepared as shown in Fig. 6. The resulting spin-polarized state has the form of a domain-wall like structure between the ψ_0 and $\psi_{\pm 1}$ components. The parameters are $\Omega = 0.1$ and $\mu = 2$. Top-right panel shows the wavefunctions of the domain-wall state found at $\mu = 1.43$. Bottom panel: the norm of each component in the above-mentioned domain-wall structure versus the chemical potential (the dependences for $\Delta\theta = 0$ or π are identical).

tially loaded into three different traps, $V_j(x)$, of the same strength, Ω , centered at different positions:

$$V_j(x) = \frac{1}{2}\Omega^2(x - j\Delta x)^2, \quad j = -1, 0, +1. \quad (19)$$

We choose $\Delta x = \Omega^{-1}$ (i.e., $\Delta x = 10$ for $\Omega = 0.1$), which implies initially overlapping TF configurations, see Fig. 6. After constructing this state, we turn off the traps $V_{-1}(x)$ and $V_0(x)$, retaining only the rightmost one, $V_{+1}(x)$, which now acts on all the three components, and feed the initial configuration state into the fixed-point algorithm, to find new spin-polarized states. Other possibilities, such as turning off potentials $V_{\pm 1}$ and keeping V_0 , arranging the three components in a different way, etc., eventually lead to retrieving the spin-polarized states presented in the previous sections, while the approach outlined above [keeping $V_{+1}(x)$ and switching $V_{-1}(x)$ and $V_0(x)$ off] generates new DW patterns, which are displayed in Fig. 7, and could not be obtained otherwise. (The asymmetry of the procedure is instrumental in generating the new states).

The most interesting spin-polarized DW states found following this procedure correspond to values of the chemical potential $\mu \geq 1.43$ (or norm $N \geq 5400$ for $\Omega = 0.1$); for smaller values of μ we typically find structures of the Thomas-Fermi type. Two examples, one for $\mu > 1.43$, and another corresponding to $\mu = 1.43$, are shown in Fig. 7. In the former one, the ψ_0 component

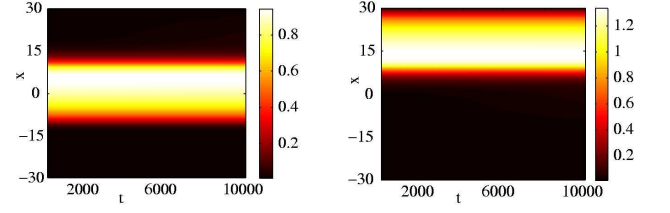


FIG. 8: (Color online) Evolution of the domain-wall structure shown in the top-left panel of Fig. 6, to which a random perturbation was added. Shown in the left and right panels are spatiotemporal contour plots of the densities of components $\psi_{\pm 1}$ (identical ones) and ψ_0 , respectively.

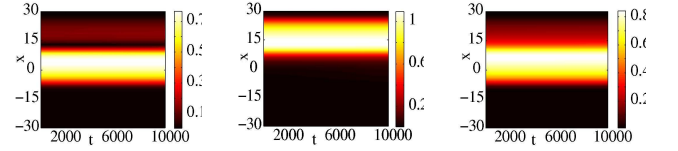


FIG. 9: (Color online) Same as Fig. 8 but for the state shown in the top-right panel of Fig. 6. The left, middle and right panels show, respectively, the densities of ψ_{-1} , ψ_0 and ψ_{+1} . Noteworthy is a stationary dark-soliton-like structure, located at $x \approx 13$ in the ψ_{-1} component.

(which has the larger norm) is centered to the right of the midpoint of the remaining trap ($x_{+1} = 10$), while the identical $\psi_{\pm 1}$ components are pushed to the left, due to the repulsion from ψ_0 , with a DW created between $\psi_{\pm 1}$ and ψ_0 . Figure 7 displays an example of such a DW structure for $\mu = 2$ and $\Omega = 0.1$.

The state found at the above-mentioned value, $\mu = 1.43$, is shown in the top-right panel of Fig. 7, for $\Delta\theta = 0$. In this state, the shape of the ψ_0 component is similar to that considered above, while the $\psi_{\pm 1}$ components are *not* identical, in contrast to the above example. In this case the ψ_0 and $\psi_{\pm 1}$ components overlap over a wider spatial region. Note that ψ_{-1} changes its sign at $x \approx 13$, featuring a structure resembling the waveform of a dark soliton embedded in a bright one [21].

The stability of the DW states was also investigated by means of the BdG equations. It was concluded that there are no eigenvalues with a real part in the interval $1.43 \leq \mu \leq 5$, or, equivalently, $5400 \leq N \leq 35000$ for $\Omega = 0.1$ (not shown here in detail). Thus, the DWs are stable in this region. Verification of the stability, performed by direct simulations of Eqs. (4) and (5), is illustrated in Figs. 8 and 9, for $\mu = 2$ and $\mu = 1.43$, respectively. It is obvious that these states are indeed stable, for very large times exceeding $t = 10000$ (i.e., 12 seconds in physical units).

VI. CONCLUSIONS

In this work, we have studied spin-polarized states in anti-ferromagnetic spinor ($F = 1$) Bose-Einstein condensates. In particular, our analysis applies to a quasi-1D spinor condensate of sodium atoms. The considerations were based on analytical calculations and numerical computations of the coupled Gross-Pitaevskii equations for this setting.

Assuming that all three hyperfine (spin) components are confined in the same harmonic trap, we have found various types of spin-polarized states and examined their stability. The first family consists of Thomas-Fermi configurations, considered analytically in the framework of the single-mode approximation (which assumes the similarity of the spatial profiles of all the components). Within their existence region, these states were found to be stable. Also identified were more complex patterns, which include states composed of pulse-like structures in one component, which induce holes in the other components, and states with holes in all three components. These states feature windows of weak instability. The development of the instability was investigated by means of direct numerical simulations, which demonstrate that it manifests itself at very long times, and results in a weak deformation of the states with a single hole in some of the components, and a stronger one in the states with holes in all components.

Fully stable families of spin-polarized states develop

from initial configurations which are initially separated (by means of three different traps) components. These states form domain-wall structures between the components, at values of the chemical potential above a critical value. At the critical value (corresponding to a certain norm, for a fixed trap's strength), we have found another spin-polarized state (including a dark-soliton element), in which all the components partly overlap.

It would clearly be interesting to investigate the existence and stability of higher-dimensional counterparts of the 1D spin-polarized states found in this work. Another relevant question for further analysis is whether such spinor condensates support stable topological objects, such as dark solitons or vortices. Work in these directions is in progress.

The work of H.E.N. and D.J.F. was partially supported from the Special Research Account of University of Athens. H.E.N. acknowledges partial support from EC grants PYTHAGORAS I. P.G.K. acknowledges support from NSF-CAREER, NSF-DMS-0505663 and NSF-DMS-0619492, as well as the warm hospitality of MSRI during the initial stages of this work. The work of B.A.M. was supported, in a part, by the Israel Science Foundation through the Center-of-Excellence grant No. 8006/03, and the German-Israel Foundation through Grant No. 149/2006. R.C.G. acknowledges support from NSF-DMS-0505663. Work at Los Alamos National Laboratory is supported by the USDoe.

-
- [1] D. M. Stamper-Kurn and W. Ketterle, cond-mat/0005001.
 - [2] D. M. Stamper-Kurn, M. R. Andrews, A. P. Chikkatur, S. Inouye, H.-J. Miesner, J. Stenger, and W. Ketterle, Phys. Rev. Lett. **80**, 2027 (1998).
 - [3] M.-S. Chang, C. D. Hamley, M. D. Barrett, J. A. Sauer, K. M. Fortier, W. Zhang, L. You, and M. S. Chapman, Phys. Rev. Lett. **92**, 140403 (2004).
 - [4] J. Stenger, S. Inouye, D. M. Stamper-Kurn, H.-J. Miesner, A. P. Chikkatur, and W. Ketterle, Nature (London) **396**, 345 (1998).
 - [5] A. E. Leanhardt, Y. Shin, D. Kielpinski, D. E. Pritchard, and W. Ketterle, Phys. Rev. Lett. **90**, 140403 (2003).
 - [6] J. Ieda, T. Miyakawa, and M. Wadati, Phys. Rev. Lett. **93**, 194102 (2004); J. Phys. Soc. Jpn. **73**, 2996 (2004).
 - [7] L. Li, Z. Li, B. A. Malomed, D. Mihalache, and W. M. Liu, Phys. Rev. A **72**, 033611 (2005).
 - [8] W. Zhang, Ö. E. Müstecaplıoglu, and L. You, Phys. Rev. A **75**, 043601 (2007).
 - [9] M. Uchiyama, J. Ieda, and M. Wadati, J. Phys. Soc. Jpn. **75**, 064002 (2006).
 - [10] B. J. Dabrowska-Wüster, E. A. Ostrovskaya, T. J. Alexander, and Y. S. Kivshar, Phys. Rev. A **75**, 023617 (2007).
 - [11] H. E. Nistazakis, D. J. Frantzeskakis, P. G. Kevrekidis, B. A. Malomed, and R. Carretero-González, arXiv:0705.1324.
 - [12] H. Pu, C. K. Law, S. Raghavan, J. H. Eberly, N. P. Bigelow, Phys. Rev. A **60**, 1463 (1999); H. Pu, S. Raghavan, and N. P. Bigelow, Phys. Rev. A **61**, 023602 (2000).
 - [13] T.-L. Ho, Phys. Rev. Lett. **81**, 742 (1998).
 - [14] S. Yi, Ö. E. Müstecaplıoglu, C. P. Sun, and L. You, Phys. Rev. A **66**, 011601(R) (2002).
 - [15] N. P. Robins, W. Zhang, E. A. Ostrovskaya, and Y. S. Kivshar, Phys. Rev. A **64**, 021601(R) (2001).
 - [16] V. M. Pérez-García, H. Michinel, and H. Herrero, Phys. Rev. A **57**, 3837 (1998); L. Salasnich, A. Parola, and L. Reatto, Phys. Rev. A **65**, 043614 (2002); *ibid.* **66**, 043603 (2002).
 - [17] T. Ohmi and K. Machida, J. Phys. Soc. Jpn. **67**, 1822 (1998).
 - [18] E. G. M. van Kempen, S. J. J. M. F. Kokkelmans, D. J. Heinzen, and B. J. Verhaar, Phys. Rev. Lett. **88**, 093201 (2002).
 - [19] N. N. Klausen, J. L. Bohn, and C. H. Greene, Phys. Rev. A **64**, 053602 (2001).
 - [20] L. P. Pitaevskii and S. Stringari, *Bose-Einstein Condensation* (Oxford University Press, Oxford, 2003).
 - [21] P. G. Kevrekidis, D. J. Frantzeskakis, B. A. Malomed, A. R. Bishop, and I. G. Kevrekidis, New J. Phys. **5**, 64.1 (2003).